ADVANCED FUNCTIONAL MATERIALS
www.afm-journal.de

Aligned Carbon Nanotube–Based Flexible Gel Substrates for Engineering Biohybrid Tissue Actuators

Su Ryon Shin, Courtney Shin, Adnan Memic, Samaneh Shadmehr, Mario Miscuglio, Hyun Young Jung, Sung Mi Jung, Hojae Bae, Ali Khademhosseini, Xiaowu (Shirley) Tang, and Mehmet R. Dokmeci**

Muscle-based biohybrid actuators have generated significant interest as the future of biorobotics but so far they move without having much control over their actuation behavior. Integration of microelectrodes into the backbone of these systems may enable guidance during their motion and allow precise control over these actuators with specific activation patterns. Here, this challenge is addressed by developing aligned carbon nanotube (CNT) forest microelectrode arrays and incorporating them into scaffolds for cell stimulation. Aligned CNTs are successfully embedded into flexible and biocompatible hydrogels exhibiting excellent anisotropic electrical conductivity. Bioactuators are then engineered by culturing cardiomyocytes on the CNT microelectrode-integrated hydrogel constructs. The resulting cardiac tissue shows homogeneous cell organization with improved cell-to-cell coupling and maturation, which is directly related to the contractile force of muscle tissue. This centimeter-scale bioactuator has excellent mechanical integrity, embedded microelectrodes, and is capable of spontaneous actuation behavior. Furthermore, it is demonstrated that a biohybrid machine can be controlled by an external electrical field provided by the integrated CNT microelectrode arrays. In addition, due to the anisotropic electrical conductivity of the electrodes provided by aligned CNTs, significantly different excitation thresholds are observed in different configurations such as the ones with electrical fields applied in directions parallel versus perpendicular to the CNT alignment.

1. Introduction

Nature can be an inspiration to develop innovative methods aimed at solving medical, environmental, and engineering challenges.[1] In particular, using muscle tissue as an inspiration, tissue-engineering approaches can be used to build biological machines.[2] Furthermore, since they are built from cells, these biological machines are capable of dynamically sensing and adapting to environmental cues including responding to externally applied stimuli. These devices and actuators could be used to handle numerous challenges specifically for in vitro biological applications, including drug screening and biorobotics.[3] Fabricating contractile muscular tissues (vasculature, skeletal, and cardiac muscles)[4] and integrating them with adaptable soft materials can allow for deformation, locomotion, and control with greater degrees of freedom. These systems can be combined in a simple, low-power,

Dr. S. R. Shin, C. Shin, M. Miscuglio, Prof. A. Khademhosseini, Dr. M. R. Dokmeci
Biomaterials Innovation Research Center
Department of Medicine
Brigham and Women's Hospital
Harvard Medical School
Boston, MA 02139, USA
E-mail: mdokmeci@rics.bwh.harvard.edu

Dr. S. R. Shin, C. Shin, M. Miscuglio,
Prof. A. Khademhosseini, Dr. M. R. Dokmeci
Harvard-MIT Division of Health Sciences and Technology
Massachusetts Institute of Technology
Cambridge, MA 02139, USA

Dr. S. R. Shin, Prof. A. Khademhosseini, Dr. M. R. Dokmeci
Wyss Institute for Biologically Inspired Engineering
Harvard University
Boston, MA 02115, USA

Prof. A. Memic
Center of Nanotechnology
King Abdulaziz University
Jeddah 21589, Saudi Arabia

S. Shadmehr, Prof. X. (Shirley) Tang
Department of Chemistry and Waterloo Institute for Nanotechnology
University of Waterloo
200 University Ave. West, Waterloo, Ontario N2L 3G1, Canada
E-mail: tangxw@uwaterloo.ca

Prof. H. Y. Jung
Department of Energy Engineering
Gyeongnam National University of Science and Technology
Jinju, Gyeongnam 660-758, Republic of Korea

Dr. S. M. Jung
Department of Electrical Engineering and Computer Science
Massachusetts Institute of Technology
Cambridge, MA 02139, USA

Prof. H. Bae
College of Animal Bioscience and Technology
Department of Bioindustrial Technologies
Konkuk University
Hwayang-dong, Kwangjin-gu, Seoul 143-701, Korea

Prof. A. Khademhosseini
Department of Physics
King Abdulaziz University
Jeddah 21569, Saudi Arabia

Prof. A. Khademhosseini
Department of Maxillofacial Biomedical Engineering and Institute of Oral Biology
School of Dentistry
Kyung Hee University
Seoul 130-701, Republic of Korea

DOI: 10.1002/adfm.201501379

and cost-effective platform when compared to systems made using conventional robotics composed of metallic and electroactive polymeric structures.[5] Recent advances in engineering cardiac tissues in vitro has led to devices with strong spontaneous contractile behavior allowing more precisely controlled actuation from external signal sources (i.e., electrical or optical stimulation).[6,7] These advantageous properties of cardiac muscle have inspired the development of biological machines that include cantilevers,[8] muscular thin film–based biohybrid actuators,[9] crab-like robots,[10] jellyfish,[11] self-propelled swimming robots,[12] and walking "biological biomorph" cantilevers at the millimeter scale.[13] However, despite significant technological advances, developing biological machines capable of long-term operation with reproducible and precise control over their direction within a biological environment remains a challenge.

To address this and similar challenges, self-propelling biological machines can be integrated with cell stimulating mini- or microelectrodes that provide users with precise control over their actuation behavior.[7,9] Integration of electrodes onto biological machines for the purpose of external stimulation is challenging. Any direct contact between the electrodes and the biological samples, in general, may cause: a) hydrolysis of the culture medium when an applied electric potential (>±1 V) exceeds the water window and hence causes bubble formation and a localized pH gradient; b) joule heating of the medium; c) contamination of the culture medium due to products of electrode corrosion; d) surface fouling of electrodes, as a result of electrochemical reactions on the electrode surface that can further lead to damage in bioinspired constructs.[14] To circumvent some of these problems, microelectrodes or microelectrode arrays (MEA) that can provide stimulation with low electrical potentials should be used. Furthermore, microelectrodes can be fabricated on flexible substrates with precisely defined dimensions and could therefore provide a highly reproducible and well-quantified electric field over the whole tissue constructs.[15,16]

Electrical and chemical stability is a critical requirement while developing microelectrodes for tissue stimulation. Cannizzaro et al.[17] and Tandon et al.[18] have carefully studied different electrode materials, their configuration, magnitude of input voltage, and electrode aging (especially in cardiac tissue engineering), and noted that carbon can be used as an ideal electrode material. Carbon has several benefits that include high capacitance, fast charge transfer, and high resistance to corrosion compared to titanium, titanium nitride, and stainless steel.[19] However, a pair of carbon rod electrodes is difficult to integrate onto flexible microporous substrates due to their large size and rigid behavior. As an alternative to carbon, electrodes based on carbon nanotubes (CNTs) are promising candidates and are amenable for easy integration into biological machines. Previously, CNTs have been shown to possess favorable biocompatibility, fibrous morphology, flexibility, high electrical and mechanical properties, strong tissue adhesion, and possess optimal long-term stimulation ability in contrast to conventional metallic electrodes.[20] More recently, aligned CNTs were used to fabricate wearable and stretchable devices with high durability, fast response, and low creep.[21,22] Similarly, vertically aligned CNT microelectrode arrays are emerging materials with numerous attractive properties for stimulation of biohybrid actuators. For example, they can be used to generate electric fields using low potentials to induce cell polarization. Despite their advantages, few efforts have been made to integrate them into substrates for creating flexible biological machines.

In our previous work, we have observed that the use of CNT-methacrylol modified gelatin (GelMA) conductive gels enhanced the beating behavior of cardiomyocytes.[23,24] The cells began to beat in a shorter timeframe, maintained their beating activity for a longer time and had more stable beating patterns. The pacing of the cells was done via external carbon rod or Pt wire electrodes placed far away from the cells inside a culture dish. In the current study, we have created a smart substrate with integrated pacing electrodes. To make the electrodes, rather than using dispersed CNTs inside the gels, which cannot be used for stimulation, we used an alternate strategy. The advantage of this system is twofold, first, it allows pacing in close contact to the cells which allowed the use of lower pacing voltages. In addition, since the signals can be applied to specific regions of the biohybrid actuator, the platform enables localized stimulation and hence guidance which will be shown at another study. Generation of embedded, mechanically flexible, and patternable microelectrodes within a tissue construct is an important first step toward future implementation of robotic systems with more complex actuation behaviors. The vertically aligned CNT microelectrode forest arrays were explored for this purpose. The ability to integrate them into cell friendly hydrogel substrates enables novel applications in remotely controlled biohybrid actuators in the future.

Here, we introduce an innovative approach to fabricate and integrate vertically aligned CNT microelectrode arrays into flexible cardiac muscle tissue constructs. After growing vertically aligned CNT forest microelectrode arrays on silicon substrates, they were transferred to hydrogel substrates. Next, a hybrid conductive hydrogel substrate was created by dispersing individual CNTs inside a thin layer of GelMA. Then, this layer was bonded onto the hydrogel sheet containing CNT forest microelectrodes. The CNT forest–based microelectrode arrays were sandwiched between two thin hydrogel layers to prevent undesirable CNT delamination and to improve the mechanical stability of the construct. The CNT-GelMA hybrid hydrogel surface was used as the cell culture substrate to induce maturation of cardiac muscle tissues.[1,23,24] The resulting 3D biohybrid constructs showed excellent mechanical integrity with embedded microelectrode arrays and advanced electrophysiological functions with strong muscle contraction. Therefore, we successfully created a 3D biohybrid actuator with controllable actuation and movement under an electrical field generated by integrated electrodes.

2. Results and Discussion

2.1. Design of 3D Bioelectronics System

The multilayer engineered cardiac tissue constructs incorporating vertically aligned CNT forest microelectrode arrays were fabricated according to the process described in **Figure 1**. First, a vertically aligned CNT forest microelectrode array was

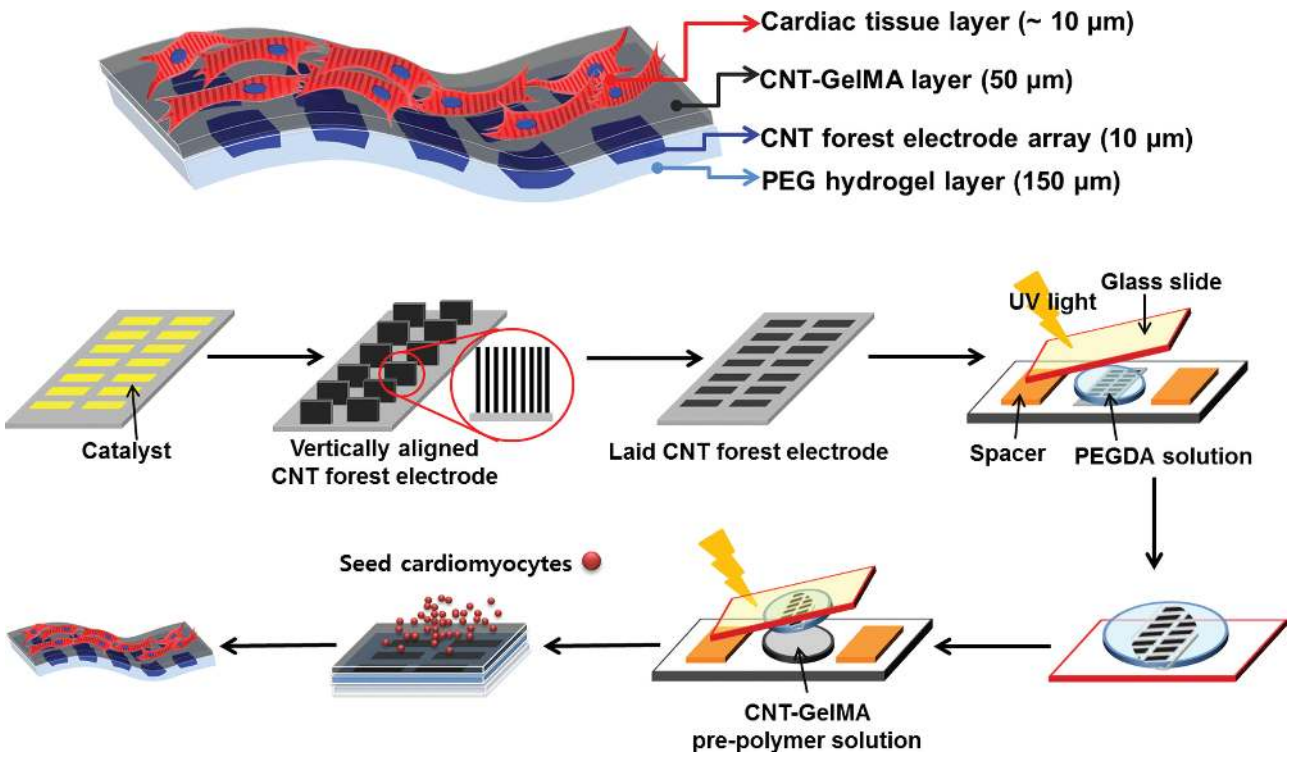

Figure 1. A schematic illustrating the fabrication steps to produce 3D biohybrid actuators composed of cardiac tissue on top of a multilayer hydrogel sheet impregnated with aligned CNT microelectrodes.

fabricated on a patterned Si wafer by a chemical vapor deposition (CVD) process. The development of biomimetic substrates that are amenable to electrode integration and emulate the properties of the muscle tissue is of great importance for successfully creating muscle-based biological machines. 3D hydrogels are excellent candidates to create biomimetic substrates due to their ability to control physical and chemical properties with their high permeability for the transport of nutrients and metabolites. Before being transferred to hydrogel substrates, vertically aligned CNT forests on Si wafers were first dipped into deionized (DI) water briefly, pulled out, and air dried. After this process, the vertical CNT forests were flattened onto Si substrates using elastocapillary induced densification.[25] The transfer of CNT forests onto hydrogels was performed by dispensing a solution of PEG prepolymer onto the Si wafer, and curing the prepolymer with UV light, which formed a nondegradable and biocompatible hydrogel. By peeling the poly(ethylene glycol) diacrylate (PEGDA) layer from the Si substrate, the transfer process was completed and a PEG hydrogel layer with embedded CNT electrode array was successfully obtained with high reproducibility. To provide a biochemical environment suitable for cardiac tissue culture, we dispensed and UV crosslinked the 50 μm thick CNT-GelMA hydrogel layer over the PEG/CNT microelectrode array composite layer. At the end of this process, we created a two-layer hydrogel structure where the 50 μm thick CNT-GelMA hydrogel layer was residing on top of the 150 μm thick CNT forest–based microelectrode array. Finally, neonatal rat cardiomyocytes were cultured on the CNT-GelMA side of the multilayer structure to yield a 3D hybrid bioactuating construct. The advantage of this stepwise, bottom-up approach is that it allowed for minimally invasive integration of electronic devices with cell and extracellular matrix (ECM) components at the cellular level in 2D and 3D.

2.2. Vertically Aligned CNT Forest Microelectrode Arrays with Anisotropic Electrical Property

We designed and fabricated thin, microscale CNT forest electrode arrays in order to: a) generate an efficient electric field for cultured cells on hydrogels; b) compensate for physical constraints created by electrode presence, which can limit muscle actuation; and c) allow for easy integration into soft biomaterial layers.[26] Vertically aligned CNT arrays were grown on an iron catalyst patterned Si wafer by CVD using ethylene as the carbon source at 800 °C (Figure S1, Supporting Information). In addition, the length and diameter of CNTs could be easily controlled by changing the reaction time, size of catalyst, and other synthesis conditions. **Figure 2**a,b shows a tilted scanning electron microscope (SEM) image of well-defined thin film arrays with uniform alignment along the growth direction. The dimensions of each CNT forest, i.e., CNT microelectrode, were measured to be 460 μm (width), 300 μm (height), and 50 μm (thick). The array of microelectrodes was spaced 200 μm apart in order to be able to induce spontaneous beating, changes in repolarization characteristics and conduction path and velocity. This design is similar to those used in commercially available MEA designs.[27] Unlike the solid metallic electrodes used in MEAs, the CNT microelectrodes can maintain the flexibility of the final construct after electrode integration.[15] The CNT forests

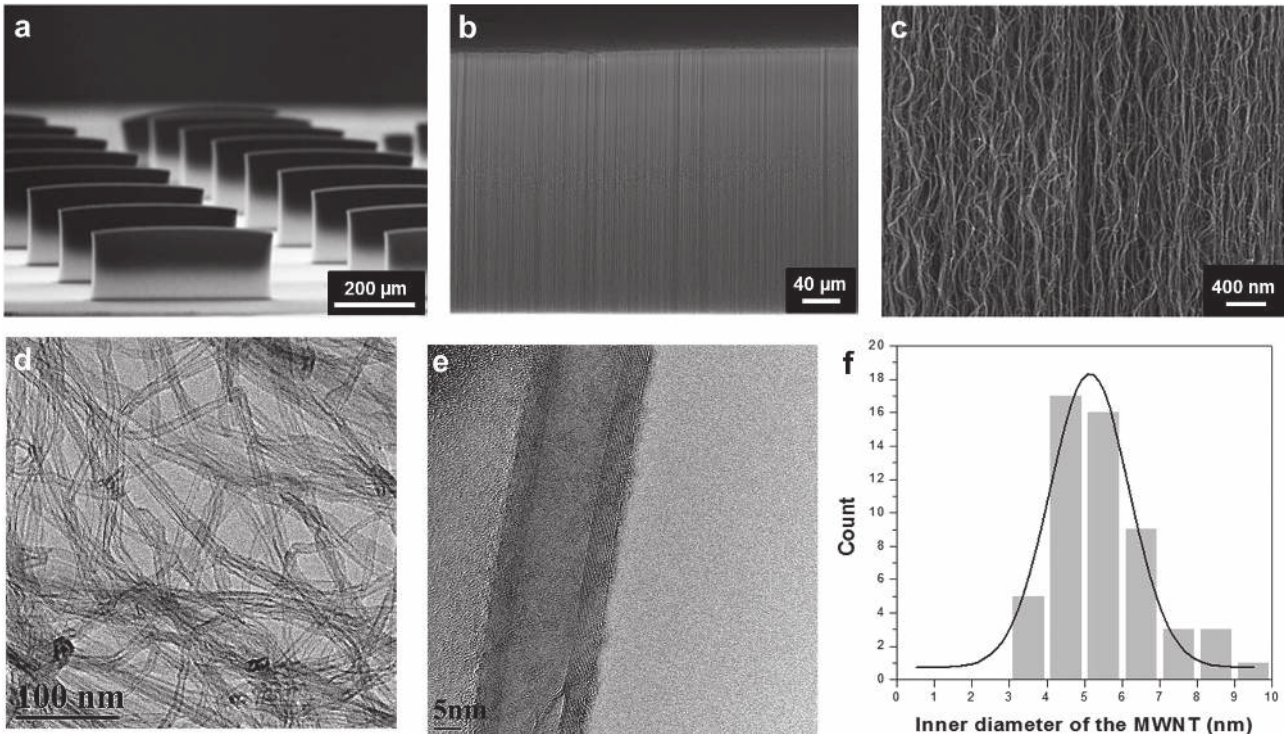

Figure 2. SEM images of a) vertically aligned CNT forests (width: 460 μm and height: 300 μm), b,c) magnified parts of the CNT forest surface. d,e) HRTEM images of multiple and individual MWNTs isolated from the CNT forest. f) Diameter distribution of the MWNTs in the CNT forests.

showed a visually discernible morphology with high tortuosity and a 3D interconnected network of nanotubes (Figure 2c). To characterize the diameter distribution of CNTs inside the CNT forests, we analyzed the samples by high-resolution transmission electron microscopy (HRTEM). Figure 2d,e shows homogeneous shape and size distribution of multiwall nanotubes. The inner diameter and the wall thickness of the nanotubes were around 5 and 2 nm (Figure 2f) with a narrow distribution. In addition, these forest-based conductive materials have been shown to exhibit high electrical conductivity with small amount of nanotube loading and highly reversible electrical property changes under 20% strain change.[22,28] Therefore, vertically aligned CNT forests represent a unique conducting material made up of nanotube networks with a resilient structural retention that could provide stable electrical conductivity under muscle contraction and deformation.

A key electrical conductivity indicator of the embedded microelectrodes is their ability to sustain pacing of cardiac tissue. To measure the conductivity of vertically aligned CNT electrodes, they were first flattened onto the Si wafer where they maintained their alignment in the lateral direction (Figure S2, Supporting Information). Elastocapillary densification resulted in an increased array density, reducing the layer thickness down to 10 μm. Next, Au contacts were deposited on both sides of flattened CNT forests in order to obtain robust electrical measurements, as shown in **Figure 3** (right panel). Also shown in Figure 3 (left panel) are the *I*–*V* curves measured in configurations parallel and perpendicular to the alignment direction of CNTs. Conductivity parallel to the direction of CNT alignment (12.1 S cm^{-1}) was three times higher than that of the one along the perpendicular direction (3.5 S cm^{-1}). The parallel direction has enhanced conduction pathways relative to the perpendicular direction, resulting in the electrical anisotropy. The alignment of CNTs (either in the perpendicular direction or the parallel direction to the applied voltage) was the primary cause of the anisotropic conductivity of the fabricated constructs. Therefore, the unique electrical properties of CNT forest microelectrodes, especially when compared to other metal based alternatives, might better mimic the anisotropic conductivity present in the fiber structure of the cardiac muscle tissue.

2.3. Integration of Vertically Aligned CNT Forest Microelectrode Arrays into Hydrogel Layers

Previous studies have relied on poly(methyl methacrylate) (PMMA), polyethylenimine (PEI), or polydimethylsiloxane (PDMS)[29] materials as the primary substrates for electrode fabrication due to their tolerance of large structural deformations and ease of handling. Although these materials may be suitable for the construction of biohybrid actuators, they often lack permeability to oxygen and nutrients, which can limit their seamless 3D integration with synthetic tissues.[15] To build bioinspired synthetic muscle tissue constructs, integration of electronics must be done with 3D microporous biomaterials that resemble the mechanical and biological properties of the ECM. In this work, we tested photocrosslinkable GelMA and PEG hydrogels for the integration of microelectronics. As the first step, CNT microelectrodes fabricated on the Si wafer were directly transferred to the PEG hydrogel substrate without

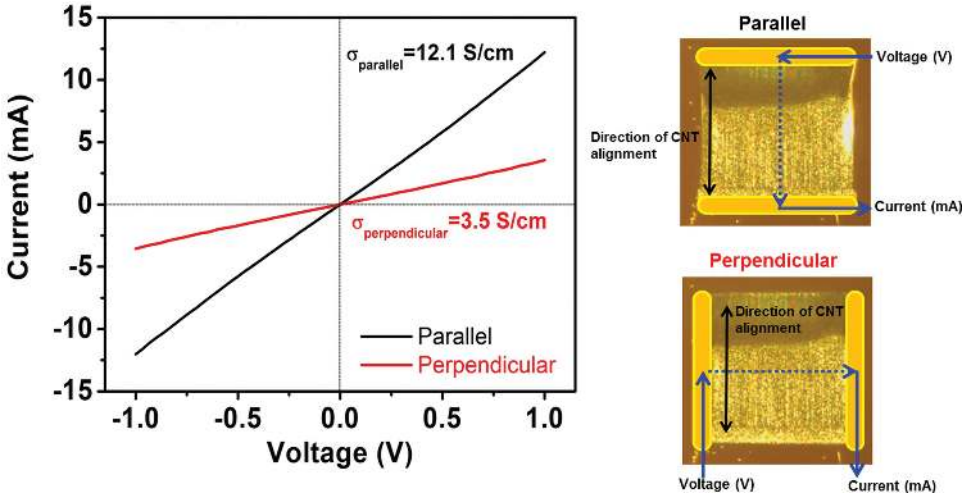

Figure 3. Two-point probe *I–V* curves from the CNT microelectrodes in parallel and perpendicular configurations relative to the nanotube alignment direction of CNT microelectrodes were measured. Au contacts were deposited at the edges of the CNT microelectrodes.

using additional sacrificial layers such as nickel coating.[15] PEG hydrogel, instead of GelMA, was used for electrode transfer because the thin GelMA hydrogel was difficult to peel off the Si wafer due to strong adhesion between GelMA and the Si surface (data not shown). Unlike previously used substrate materials, such as PMMA and PDMS, crosslinked PEG hydrogels are permeable to water, oxygen, and nutrients. In addition, they are nontoxic, nonimmunogenic, and nondegradable under physiological conditions with robust mechanical properties.[29] The transfer was achieved by dispensing a 20% PEG prepolymer solution onto the Si wafer substrate having the CNT forest arrays, followed by UV crosslinking for 50 s. In this step, PEG prepolymer solution was able to penetrate into the highly porous forest surface,[30] and hence CNTs were embedded in the PEG matrix after UV crosslinking. The flattening process broke the strong bonds between the CNT forests and the silicon substrate. Accordingly, the transfer process occurred quite seamlessly due to the weak adhesion between the flattened CNT forests and the silicon substrate. The thin PEG hydrogel film embedded with CNT forest array was readily peeled off the silicon substrate with intact electrodes (**Figure 4**a). The structural integrity, alignment, and morphology of transferred CNTs were preserved inside the 150 µm thick hydrogel layer (Figure 4b). In addition, encapsulation of the CNTs inside the PEG hydrogel prevented possible detachment of fragments or individual CNTs resulting from cracked or damaged CNT forests during contraction of the tissue constructs. To confirm cytocompatibility, cardiac fibroblasts were seeded on the CNT forest electrodes and cellular viability (i.e., LIVE/DEAD assay) was performed. The CNT forest electrodes did not display any observable cytotoxic effects to the cardiac cells since 95% cellular viability was observed in Figure 4c.

An additional CNT-GelMA hybrid hydrogel layer (thickness: 50 µm) was fabricated and placed over the PEG hydrogel layer (thickness: 150 µm) containing the CNT forest microelectrode arrays. This new conductive CNT-GelMA layer effectively sandwiched the microelectrodes at the interface between the two hydrogels. The bond between two gel layers was reinforced by the application of a UV light. Cardiomyocytes were later

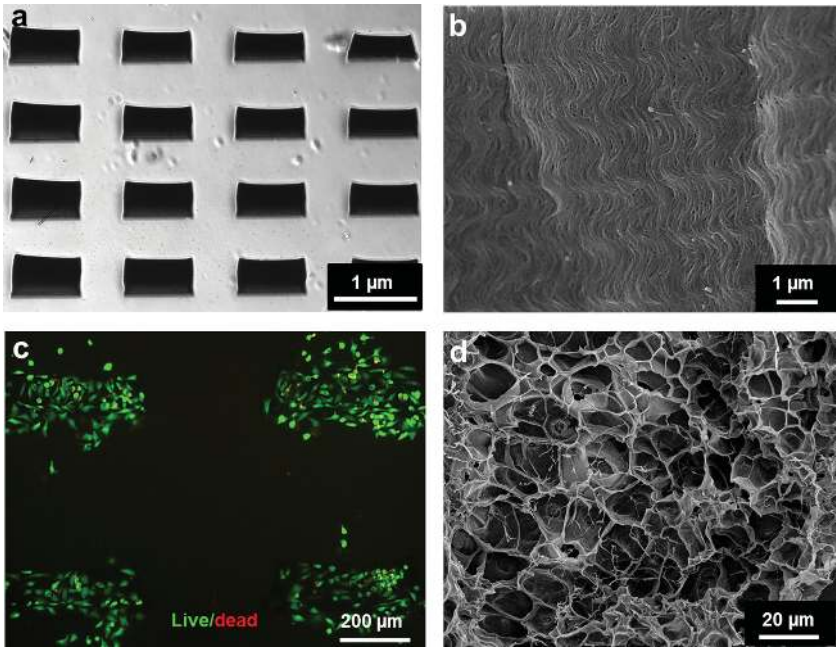

Figure 4. SEM images show that a) arrays and b) alignment of CNTs were preserved after they were transferred to the PEG substrate. c) Cardiac fibroblast cell viability using LIVE/DEAD staining after 24 h of seeding on CNT forest microelectrodes. d) SEM images show porous surfaces of a 1 mg mL^{-1} CNT-GelMA layer. This image shows nanofibrous networks of CNTs across and inside a porous gelatin framework.

seeded on the CNT-GelMA surface. Conductive CNT-GelMA hybrid hydrogel substrates have been shown previously to improve cardiac cell organization, maturation, and cell-to-cell coupling.[23] Figure 4d shows the porous surface of the CNT-GelMA (1 mg mL^{-1} concentration of CNTs in 5% GelMA) hydrogel layer. The CNT nanofibrous networks within the GelMA hydrogel layer lead to enhanced electrical conductivity and mechanical properties of the constructs.[23] It is anticipated that the CNT-GelMA would promote the formation of fully matured homogeneous cardiac tissue and offer better mechanical integrity during contraction of the tissue construct. In addition, the acrylic and acrylamide groups present on both GelMA and PEG hydrogels (i.e., PEGDA) generated covalent bonds after UV irradiation which helped minimize the risk of detachment of the two hydrogel layers. Therefore, the CNT forest microelectrode arrays were physically constrained in between two hydrogel layers and can handle cyclic deformations.

2.4. Phenotypic and Electrophysiological Characteristics of the 3D Biohybrid System

To complete the 3D biohybrid system fabrication, neonatal rat cardiomyocytes were cultured on the microelectrode-embedded multilayer hydrogel sheets for 5–8 d to form a cardiac tissue layer. The organization and phenotype of cardiomyocytes on the construct was investigated by immunostaining for cardiac biomarkers (i.e., connexin 43 (Cx-43) and sarcomeric α-actinin) after 5 d of culture. Cx-43 and sarcomeric α-actinin are involved in intercellular electrical and metabolic coupling, and muscle contraction, respectively. Fluorescence microscopy of cultured tissue revealed a high density of cardiomyocytes in close contact with the microelectrode arrays (**Figure 5**a). Cardiac tissues on these constructs possessed a well-defined, elongated, and interconnected sarcomeric α-actinin structures (Figure 5b). In addition, we also observed homogeneous distribution of Cx-43 with enhanced synchronous contractile properties of the entire cardiac tissue construct. These observations are in close agreement with previous reports from our group.[23] Furthermore, cardiac tissues located directly above the CNT forest electrodes (red dotted arrow) showed well-interconnected sarcomeric structures with Cx-43 expression that was morphologically different than the ones located directly above the open spaces in between the electrodes (yellow dotted arrow) which could be due to the higher mechanical stiffness of hybrid gels embedded with CNT forests compared to the gels having individual CNTs (Figure 5c).

Finally, the biohybrid constructs made with cardiomyocytes cultured on hydrogel sheets (square shape, 1 cm^2), were observed to spontaneously detach from the glass substrate due to constant actuation of the cells and adopted a planar shape with loosely rolled-up edges (Figure 5d). The CNT forest electrodes within multilayer hydrogel constructs were able to efficiently stimulate the cardiomyocytes and forced them to

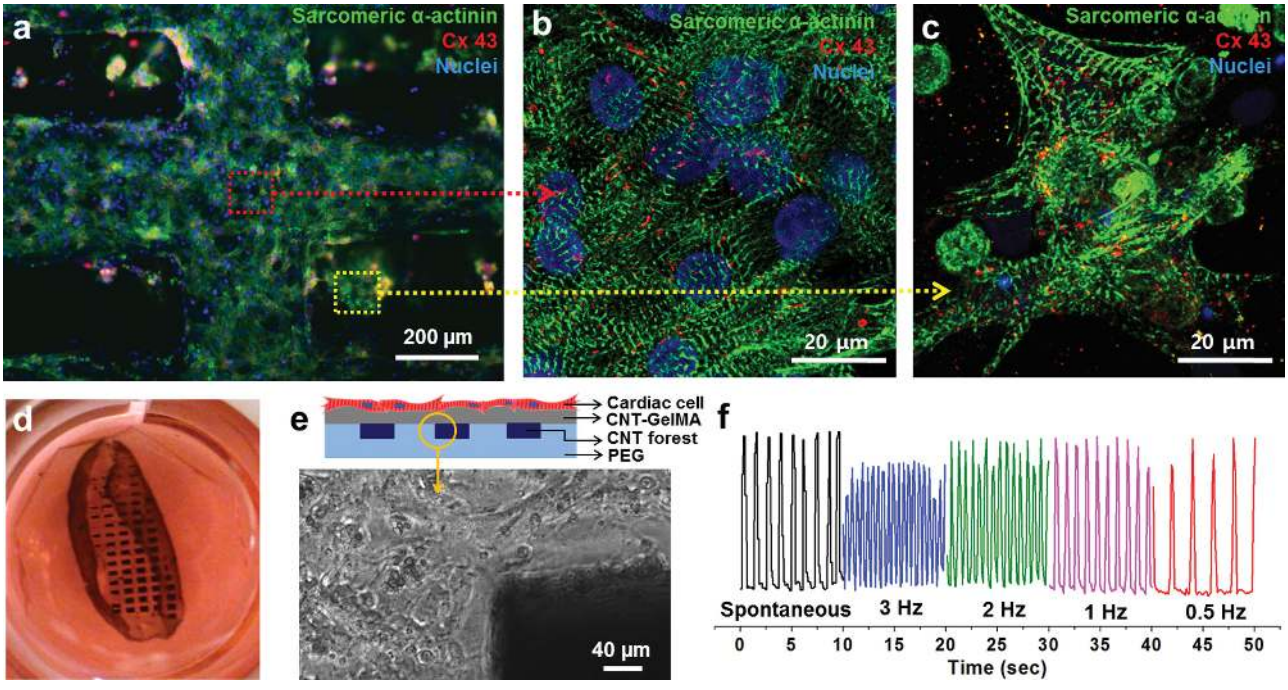

Figure 5. Cardiac tissue organization on composite hydrogel layers incorporating CNT forest electrodes. a) Phenotype of cardiac cells. Immunostaining of sarcomeric α-actinin (green), nuclei (blue), and Cx-43 (red) revealed that cardiac tissues (5 d culture) were created on top of a multilayer hydrogel sheet impregnated with aligned CNT microelectrodes. Magnified image showing the well interconnected sarcomeric structures of cardiac tissue which is located b) above locations between the electrodes (red dotted arrow) and c) above the electrodes (yellow dotted arrow). d) Photograph of a free-standing 3D biohybrid actuator cultured for 8 d. e) Schematic illustration of a multilayer hydrogel sheet impregnated with aligned CNT microelectrodes (side view). Phase contrast image of the boundary between the CNT forest electrodes and the hydrogel layer shows that the cardiac tissues remained attached to the top hydrogel layer and stayed intact. f) The displacement of the CNT forest electrode in multilayer hydrogel sheets (yellow circled tip in (b)) over time under electrical stimulation (square wave form, 1.2 V cm^{-1}, frequency: 0.5–3 Hz, 50 ms pulse width).

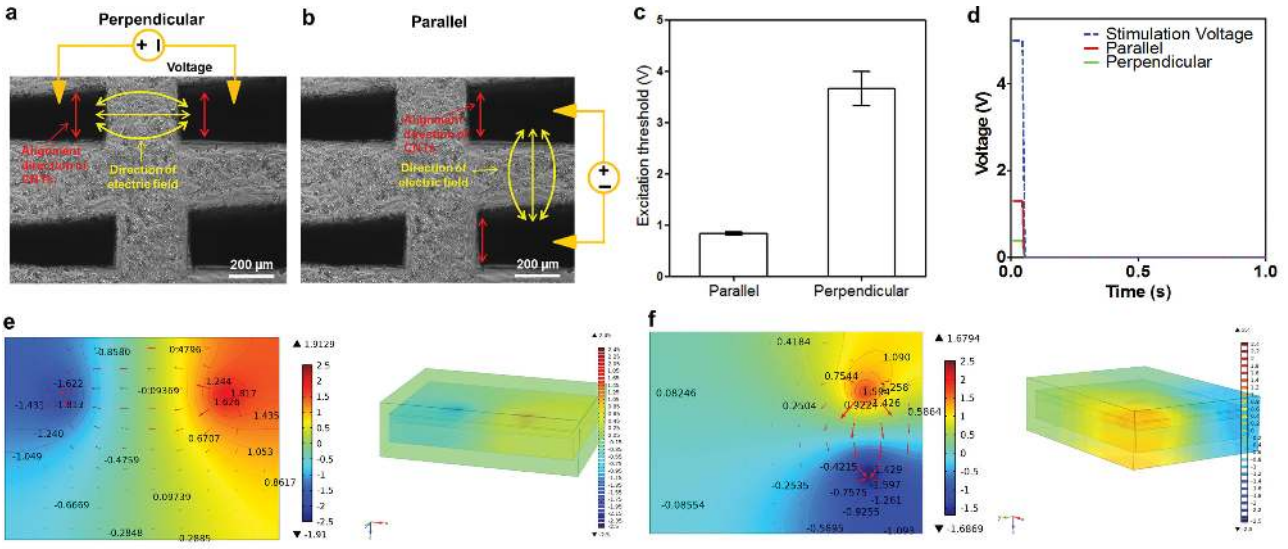

Figure 6. a,b) Phase contrast images that show the direction of the applied field which is along the parallel and the perpendicular direction to the alignment of the CNT forests. c) The excitation threshold of cardiac tissue in the parallel configuration was three times lower than that in the perpendicular configuration. d) Numerically calculated maximum voltage applied on the cardiac cell layer using the two different electrode configurations (frequency range: 0.5–3 Hz, wave: pulse signal, pulse width: 50 ms). Top views of the numerically calculated electric field applied to the muscle cells in e) perpendicular and f) parallel electrode configurations with top and cross-sectional views.

beat synchronously after only 1 d of culture. We confirmed that cardiac tissues cultured on the biohybrid actuators made on multilayer nanocomposites showed stable spontaneous beating behavior with an average beating rate of ≈108 BPM on day 8 (Movie 1). Interestingly, the average beating rate of these 3D biohybrid actuators (total thickness of the construct: ≈210 μm) showed faster beating rates compared to the rates obtained from cells cultured on CNT-GelMA hydrogels (≈50 μm thickness of whole construct and 69.8 ± 19.1 BPM on day 6).[23] In addition, the beating frequency could be precisely controlled by applying an external electric field (1.2 V cm^{-1}) at various frequencies (0.5, 1, 2, and 3 Hz, pulses with 50 ms duration) (Figure 5f, Movie 2) generated by a conventional signal generator. Therefore, we conclude that these 3D biohybrid actuators with embedded CNT forest electrodes do not significantly inhibit muscle contractile function, even though they possess higher rigidity and stiffness compared to plain hydrogels. It is expected that the CNT forest electrodes, with a Young's modulus on the order of 100 MPa to 1 GPa,[31] would have locally stiffer regions, while the overall mechanical strength of the tissue constructs would be dictated by the soft hydrogel substrates. The elastic moduli of 1.0 mg mL^{-1} CNT-GelMA and 10% PEGDA hydrogels are 23[23] and 25 kPa,[32] respectively. It is evident that the cardiac tissue layer exhibited forces strong enough to induce contraction of the whole system. Furthermore, microelectrode arrays displayed excellent mechanical integrity within 3D biohybrid actuators showing no detachment at the electrode/hydrogel interface. The constructs were able to withstand prolonged muscle tissue contraction, as shown in the phase contrast image taken on day 8 (Figure 5e). Thus, these 3D biohybrid actuator systems displayed spontaneous synchronous beating and were able to handle electrical stimulation up to 8 d in culture.

The effect of CNT forest–based microelectrode arrays with anisotropic conductivity was further investigated using a 3D biohybrid actuator (**Figure 6**). To evaluate the electrical stimulation ability of the embedded CNT forest electrodes, we have applied the electrical signals to the cells by using two CNT forest electrodes instead of the whole microelectrode array. The micromanipulator allowed us to lower the micromanipulator probes until they made contact to the CNT forest electrodes as shown in Figure S3 (Supporting Information). Compared to GelMA hydrogels these CNT forest electrodes have higher mechanical integrity and can be readily probed. During the probing step, the whole construct still maintained its mechanical integrity while the probes were lowered through a small hole on the construct until they reached the middle CNT forest electrode layer. Electrical pulse signals with different frequencies were applied to the CNT forest electrodes using a pulse generator via the micromanipulator probes. A video camera attached to a microscope with a 10× magnification was used to capture the movement of the cardiac tissue created on the multilayer construct. The beating frequency of the cardiac tissue was precisely controllable by applying an electrical signal to the CNT microelectrodes a perpendicular (Figure 6a) or parallel (Figure 6b) alignment direction, which generated an electric field perpendicular or parallel to the alignment direction of the CNTs, at different frequencies as 0.5, 1, 2, and 3 Hz. The excitation threshold which is the minimum voltage needed to induce synchronous contraction of the whole construct at each frequency was characterized for each electrode configuration. We observed that the application of the electrical signal in the direction parallel to the alignment (0.8 ± 0.03 V) resulted in drastically reduced excitation thresholds compared to those stimulated with signals applied to the electrodes aligned in the perpendicular direction (3.7 ± 0.3 V) (Figure 6c) (Movies 3 and 4). We modeled the electric field distribution generated by a pair of anisotropic CNT microelectrodes and examined the potential distribution in the parallel and perpendicular configuration (see the Supporting

Information). Furthermore, we took into account the roughness of the CNT electrode surfaces (SEM images, Figure 4b) (Figure S5, Supporting Information). The wavy nature of the CNT fibers made them act as scattering elements when the electrical field was in the direction perpendicular to the nanotube alignment. This in effect can decrease the ratio between the two (perpendicular and parallel) components of the electric field. The distribution of electrical potentials in perpendicular and parallel electrode configurations are shown in Figure 6e,f, respectively. Modeling results indicated that the drop in electrical potential was close to the microelectrodes, and also did not produce uniform electric field. Our model showed that the average potential acting on the cardiac cells significantly differed between the parallel and the perpendicular configurations (Figure 6d). When a square wave of 1 Hz at 5 V (50 ms pulse width) was applied across a pair of CNT electrodes, the potential drop across the cardiac layer was about 1.67 V in the configuration parallel to the alignment direction, which was 2.67 times (0.62 V) than the one observed in the direction perpendicular to the alignment configuration. The main reason that could explain this difference is that the spreading of the field profile occurs in parallel to the electric field even in the perpendicular configuration. In the parallel configuration, the electric field is more confined in between the pair of electrodes providing the cardiac cells with sufficient electrical field for stimulation at lower thresholds to induce beating.

3. Conclusions

In summary, we synthesized vertically aligned CNT microelectrode arrays using well-established CVD growth patterns and mechanisms. The microelectrode arrays had a 200 µm separation between each CNT forest and were next flattened on the silicon wafer breaking the bonds between the CNTs and the silicon substrate. Later, the forest arrays were successfully transferred onto mechanically stable PEG hydrogels where they were found to retain their dense array structure and structural integrity. Following transfer, we carried out *I–V* measurements in two different configurations to confirm anisotropic conductivity of the CNT electrodes. Furthermore, the CNT electrodes on a PEG substrate did not exhibit any toxicity to cells and preserved high cell viability when seeded with cardiac fibroblasts. However, neither CNT arrays nor PEG hydrogels could support cardiomyocyte adhesion. Hence an additional CNT-GelMA hybrid hydrogel layer was fabricated and was fabricated on top of the CNT forest embedded gel substrate as a cell adhesive layer. The microelectrodes were, therefore, sandwiched at the interface between two hydrogel layers, which formed covalent bonds under UV irradiation thereby crosslinking the structure, stabilizing it, and preventing delamination. Finally, the constructs were seeded with cardiomyocytes and cultured for 5–8 d and showed homogenous Cx-43 distribution and partial uniaxial alignment of sarcomeric structures. After detaching from the glass slide, the constructs spontaneously adopted a planar shape and continued their synchronous beating behavior. The constructs exhibited excellent mechanical integrity and were able to sustain spontaneous cardiomyocyte beating for long periods (8 d of culture). The beating frequency of the 3D biohybrid actuators could be precisely controlled by applying an electrical signal along the parallel and perpendicular directions relative to the alignment direction of the CNT forest at 0.5, 1, 2, and 3 Hz (at 5 V). In addition, we observed that the application of the electrical signal in the direction parallel to the CNT alignment resulted in drastically reduced excitation thresholds compared to those stimulated with a signal applied in the direction perpendicular to the CNT alignment direction. Modeling results indicated that the average voltage acting on the cardiac cells was significantly higher when the stimulating electric fields were in parallel to the alignment of CNT forest electrodes. Therefore, the high integration fidelity and unique electrical property of these CNT forest microelectrodes could be utilized to develop a growing number of diagnostic, therapeutic, and treatment tools for various cardiac, neurological, and other biomedical applications.

4. Experimental Section

Materials: High purity gases, ethylene, hydrogen, and argon (purity >99.99%) for CNT synthesis was purchased from Plaxair (Ontario, Canada). Sigma-Aldrich (Wisconsin, USA) was used as a supplier for Gelatin (Type A, 300 bloom from porcine skin), PEGDA, 3-(trimethoxysily) propyl methacrylate (TMSPMA), and methacrylic anhydride (MA). CAD Art (Washington, USA) provided the photomasks and EXPO Photonic Solutions Inc. (Ontario, Canada).

Preparation and Characterization of Vertically Aligned CNT Forest Microelectrodes: The fabrication process is illustrated in Figure 1. First, the vertically aligned CNT forest microelectrode arrays were fabricated on a Si wafer by a CVD process as described in previous reports.[25] E-beam evaporated Fe film (4 nm thick) deposited on Si/SiO_2 wafers was used as the catalyst. CVD growth was done using a gas mixture ethylene/hydrogen/argon (70:70:70 sccm) at 800 °C in a 1 in. tube furnace (Lindberg). The growth time was between 30 and 60 min with no preannealing step. Patterning of the iron catalyst films were carried out by standard photolithography using AZ3330 photoresist and LOR15A as the lift-off resist (Figure S1, Supporting Information). HRTEM images were obtained using a JEOL JEM-2010. SEM (Hitachi Model S4700, Japan) was used to assess the structure of the CNT-GelMA hybrid hydrogels. In order to determine the electrical conductivity of the CNT forest, vertically aligned CNT forests were first flattened onto the Si wafer, and then Au electrodes were coated on each side to form electrical contacts. The current–voltage (*I–V*) curves were obtained in the parallel direction and in the perpendicular direction by a two-point probe method.

Preparation and Characterization of CNT Electrode Incorporated Cardiac Tissue Constructs: Vertically aligned CNT forests were grown on Si wafers and then were dipped into DI water briefly, pulled out, and air dried. During this process, the vertically aligned CNT forests were flattened onto the Si wafer. In order to successfully create the CNT forest microelectrodes inside hydrogels, they were encapsulated between two hydrogel sheets; CNT-GelMA and PEG hydrogel layer. GelMA and CNT-GelMA hybrid hydrogels (1.0 mg mL^{-1} CNT in 5% GelMA) and PEG hydrogels were prepared based on our previously published reports.[23,33] 20% PEG prepolymer solution was dispensed onto a Si water with the CNT forest microelectrode array and crosslinked using UV light (6.9 mW cm^{-2} (360–480 nm)) and had a final thickness of 150 µm determined by a spacer. To generate a cardiac tissue actuator the CNT forest/PEG hydrogel layer was released from the Si wafer manually and placed over a CNT-GelMA prepolymer solution. The final hybrid cell culture scaffold, with a 50 µm thickness was made after exposure to UV light for 50 s which not only polymerized the gel prepolymer solution but also enhanced the attachment of CNT-GelMA to the underlying substrate. SEM (Hitachi Model S4700, Japan) was used to assess the

structure of CNT forest on the PEG hydrogel and the CNT-GelMA hybrid hydrogel. After freezing with liquid nitrogen the swollen hydrogels were lyophilized. These lyophilized samples were coated with Pt/Pd using a sputter coater for SEM imaging.

Cell Isolation and Culture: We followed well-established protocols approved by the Institute's Committee on Animal Care for isolation of neonatal rat (2 d old Sprague–Dawley) ventricular cardiomyocytes. Postextraction and enrichment via 1 h preplating, the cardiomyocytes were ready to be seeded. Culturing of seeded cells was performed in Dulbecco's modified eagle medium (DMEM, Gibco, USA) with 10% fetal bovine serum (FBS), 1% L-glutamine, and 100 units mL^{-1} penicillin–streptomycin (All from Gibco, USA) without electric field stimulation up to 8 d.

Cell Characterization: To test the cytocompatiblity of the CNT forest electrodes, they were first transferred onto a PEG hydrogel layer. Then fibronectin (50 μg mL^{-1}) was coated on this sample. A Live/Dead assay was used based on the manufacturer's instructions (Invitrogen). An inverted fluorescence microscope (Nikon, Eclipse TE 2000U, Japan) was used to collect Live/Dead images. Immunostaining of cardiac tissue constructs was performed on samples fixed for 20 min in 4% paraformaldehyde followed by a DPBS wash at room temperature. After fixation and washing, the cells were treated with 0.15% Triton X-100 in DPBS for 10 min. Finally, cell staining with a cardiac biomarker (sarcomeric α-actinin, Cx-43) was performed in the presence of a blocking buffer for 45 min at the manufacturer's suggested dilution. Similarly, a DAPI counterstain was performed at 1:20 000 dilution in DPBS for 45 min. Inverted laser scanning confocal imaging was then carried out using a confocal microscope (Leica SP5X MP, Germany).

Electrophysiological Assessment of the Biohybrid Actuators: Cultured cardiomyocytes were imaged using a microscope equipped with a CCD camera inside a temperature controlled chamber. Using a microscope with a 10× magnification (Nikon, Eclipse TE 2000U, Japan), a video camera (Sony XCD-X710) was used to capture the movement of the cells. Video capture software was used to obtain digitized beating videos with 20 frames per second (20 fps). A custom developed MATLAB code (MathWorks Inc., Natick, MA) was used for the image processing software as described in previous reports.[23,34] After 6–8 d of culture the samples detached from the substrates by themselves. Biohybrid actuators were stimulated at RT (≈20 °C) and their actuation behavior was monitored in culture medium. Panasonic HDC-HS9 digital camera (1920 × 1080 pixels, 24 fps, and recording quality) was used to capture movies of the biohybrid actuators. To assess the response of cardiomyocytes to external electrical fields, established protocols based on a modified carbon electrode system were utilized.[18] A biphasic square waveform (50 ms pulses of 0–7 V cm^{-1} at 0.5, 1, 2, and 3 Hz) was applied from an electric pulse generator to samples located between two Pt wire electrodes inside an experimentation chamber. In this setup, the samples were placed between two Pt wire electrodes (spaced ≈3 cm apart in cell culture media). To assess the stimulation ability of embedded CNT forest electrodes, the electrical signal was applied by a pair of the micromanipulation probes attached to the CNT forest electrodes which were aligned in the parallel and perpendicular directions to the applied field (Figure S3, Supporting Information). The minimum voltage needed to induce synchronous contraction (excitation threshold) at each frequency was characterized for both electrode systems.

Modeling of the Electrical Field: An analysis of the electric field profile acting on the cardiac tissue generated by an applied voltage using CNT forest electrodes is presented. The electrical field generated by the vertically aligned CNT forest microelectrodes was modeled, using commercially available software (Multiphysics, Comsol, electrostatics module) (see the Supporting Information).

Statistical Analysis: Statistical significance was performed by measuring one-way or two-way ANOVA tests (GraphPad Prism 5.02, GraphPad Software). To analyze and assess significant differences between selected treatments, Tukey's multiple comparison tests were utilized. Differences were characterized as significant for $p < 0.05$.

Supporting Information

Supporting Information is available from the Wiley Online Library or from the author.

Acknowledgements

This work was supported by the Institute for Soldier Nanotechnology, National Institutes of Health (HL092836, EB02597, AR057837, HL099073), the National Science Foundation (DMR0847287), the Office of Naval Research Young Investigator award, ONR PECASE Award, a Discovery grant fromSciences, and Engineering Research Council of Canada. The project was funded by the Deanship of Scientific Research (DSR), King Abdulaziz University, under grant no. 18-130-1434-HiCi. A.K. and A.M. therefore acknowledge with thanks DSR technical and financial support.

Received: April 7, 2015
Revised: May 7, 2015
Published online: June 12, 2015

[1] T. Dvir, B. P. Timko, D. S. Kohane, R. Langer, *Nat. Nanotechnol.* **2011**, *6*, 13.
[2] a) L. Ricotti, A. Menciassi, *Biomed. Microdevices* **2012**, *14*, 987; b) M. S. Sakar, D. Neal, T. Boudou, M. A. Borochin, Y. Li, R. Weiss, R. D. Kamm, C. S. Chen, H. H. Asada, *Lab Chip* **2012**, *12*, 4976.
[3] a) B. Yurke, A. J. Turberfield, A. P. Mills Jr., F. C. Simmel, J. L. Neumann, *Nature* **2000**, *406*, 605; b) A. Grosberg, P. W. Alford, M. L. McCain, K. K. Parker, *Lab Chip* **2011**, *11*, 4165.
[4] a) H. Herr, R. G. Dennis, *J. Neuroeng. Rehabil.* **2004**, *1*, 6; b) Y. Akiyama, T. Sakuma, K. Funakoshi, T. Hoshino, K. Iwabuchi, K. Morishima, *Lab Chip* **2013**, *13*, 4870; c) Y. Akiyama, T. Hoshino, K. Iwabuchi, K. Morishima, *PLoS One* **2012**, *7*, e38274.
[5] C. Cvetkovic, R. Raman, V. Chan, B. J. Williams, M. Tolish, P. Bajaj, M. S. Sakar, H. H. Asada, M. T. Saif, R. Bashir, *Proc. Natl. Acad. Sci. U.S.A.* **2014**, *111*, 10125.
[6] G. Vunjak-Novakovic, N. Tandon, A. Godier, R. Maidhof, A. Marsano, T. P. Martens, M. Radisic, *Tissue Eng. Part B* **2010**, *16*, 169.
[7] Z. Jia, V. Valiunas, Z. Lu, H. Bien, H. Liu, H. Z. Wang, B. Rosati, P. R. Brink, I. S. Cohen, E. Entcheva, *Circ. Arrhythm. Electrophysiol.* **2011**, *4*, 753.
[8] J. Xi, J. J. Schmidt, C. D. Montemagno, *Nat. Mater.* **2005**, *4*, 180.
[9] A. W. Feinberg, A. Feigel, S. S. Shevkoplyas, S. Sheehy, G. M. Whitesides, K. K. Parker, *Science* **2007**, *317*, 1366.
[10] J. Kim, J. Park, S. Yang, J. Baek, B. Kim, S. H. Lee, E. S. Yoon, K. Chun, S. Park, *Lab Chip* **2007**, *7*, 1504.
[11] J. C. Nawroth, H. Lee, A. W. Feinberg, C. M. Ripplinger, M. L. McCain, A. Grosberg, J. O. Dabiri, K. K. Parker, *Nat. Biotechnol.* **2012**, *30*, 792.
[12] B. J. Williams, S. V. Anand, J. Rajagopalan, M. T. Saif, *Nat. Commun.* **2014**, *5*, 3081.
[13] a) V. Chan, K. Park, M. B. Collens, H. Kong, T. A. Saif, R. Bashir, *Sci. Rep.* **2012**, *2*, 857; b) V. Chan, J. H. Jeong, P. Bajaj, M. Collens, T. Saif, H. Kong, R. Bashir, *Lab Chip* **2012**, *12*, 88.
[14] S. Ahadian, J. Ramon-Azcon, S. Ostrovidov, G. Camci-Unal, H. Kaji, K. Ino, H. Shiku, A. Khademhosseini, T. Matsue, *Biomed. Microdevices* **2013**, *15*, 109.
[15] B. Tian, J. Liu, T. Dvir, L. Jin, J. H. Tsui, Q. Qing, Z. Suo, R. Langer, D. S. Kohane, C. M. Lieber, *Nat. Mater.* **2012**, *11*, 986.
[16] a) D. H. Kim, R. Ghaffari, N. Lu, J. A. Rogers, *Annu. Rev. Biomed. Eng.* **2012**, *14*, 113; b) D. H. Kim, N. Lu, R. Ma, Y. S. Kim, R. H. Kim, S. Wang, J. Wu, S. M. Won, H. Tao, A. Islam, K. J. Yu,

T. I. Kim, R. Chowdhury, M. Ying, L. Xu, M. Li, H. J. Chung, H. Keum, M. McCormick, P. Liu, Y. W. Zhang, F. G. Omenetto, Y. Huang, T. Coleman, J. A. Rogers, *Science* **2011**, *333*, 838.

[17] C. Cannizzaro, N. Tandon, E. Figallo, H. Park, S. Gerecht, M. Radisic, N. Elvassore, G. Vunjak-Novakovic, *Methods Mol. Med.* **2007**, *140*, 291.

[18] N. Tandon, C. Cannizzaro, P. H. Chao, R. Maidhof, A. Marsano, H. T. Au, M. Radisic, G. Vunjak-Novakovic, *Nat. Protoc.* **2009**, *4*, 155.

[19] N. Tandon, A. Marsano, R. Maidhof, L. Wan, H. Park, G. Vunjak-Novakovic, *J. Tissue Eng. Regener. Med.* **2011**, *5*, e115.

[20] a) G. Cellot, E. Cilia, S. Cipollone, V. Rancic, A. Sucapane, S. Giordani, L. Gambazzi, H. Markram, M. Grandolfo, D. Scaini, F. Gelain, L. Casalis, M. Prato, M. Giugliano, L. Ballerini, *Nat. Nanotechnol.* **2008**, *4*, 126; b) L. Bareket-Keren, Y. Hanein, *Front. Neural Circuits* **2012**, *6*, 122.

[21] J. Foroughi, G. M. Spinks, G. G. Wallace, J. Oh, M. E. Kozlov, S. Fang, T. Mirfakhrai, J. D. Madden, M. K. Shin, S. J. Kim, R. H. Baughman, *Science* **2011**, *334*, 494.

[22] T. Yamada, Y. Hayamizu, Y. Yamamoto, Y. Yomogida, A. Izadi-Najafabadi, D. N. Futaba, K. Hata, *Nat. Nanotechnol.* **2011**, *6*, 296.

[23] S. R. Shin, S. M. Jung, M. Zalabany, K. Kim, P. Zorlutuna, S. B. Kim, M. Nikkhah, M. Khabiry, M. Azize, J. Kong, K. T. Wan, T. Palacios, M. R. Dokmeci, H. Bae, X. S. Tang, A. Khademhosseini, *ACS Nano* **2013**, *7*, 2369.

[24] a) T. Dvir, B. P. Timko, M. D. Brigham, S. R. Naik, S. S. Karajanagi, O. Levy, H. Jin, K. K. Parker, R. Langer, D. S. Kohane, *Nat. Nanotechnol.* **2011**, *6*, 720; b) S. R. Shin, B. Aghaei-Ghareh-Bolagh, X. Gao, M. Nikkhah, S. M. Jung, A. Dolatshahi-Pirouz, S. B. Kim, S. M. Kim, M. R. Dokmeci, X. S. Tang, A. Khademhosseini, *Adv. Funct. Mater.* **2014**, *24*, 6136.

[25] M. Mazloumi, S. Shadmehr, Y. Rangom, L. F. Nazar, X. S. Tang, *ACS Nano* **2013**, *7*, 4281.

[26] S. Ahadian, J. Ramon-Azcon, M. Estili, X. Liang, S. Ostrovidov, H. Shiku, M. Ramalingam, K. Nakajima, Y. Sakka, H. Bae, T. Matsue, A. Khademhosseini, *Sci. Rep.* **2014**, *4*, 4271.

[27] B. Liau, D. Zhang, N. Bursac, *Regener. Med.* **2012**, *7*, 187.

[28] P. P. Abadi, S. B. Hutchens, J. R. Greer, B. A. Cola, S. Graham, *Nanoscale* **2012**, *4*, 3373.

[29] Y. Wang, R. Yang, Z. Shi, L. Zhang, D. Shi, E. Wang, G. Zhang, *ACS Nano* **2011**, *5*, 3645.

[30] M. K. Shin, J. Oh, M. Lima, M. E. Kozlov, S. J. Kim, R. H. Baughman, *Adv. Mater.* **2010**, *22*, 2663.

[31] M. F. L. D. Volder, S. J. Park, S. H. Tawfick, D. O. Vidaud, H. A. John, *J. Micromech. Microeng.* **2011**, *21*, 12.

[32] C. B. Hutson, J. W. Nichol, H. Aubin, H. Bae, S. Yamanlar, S. Al-Haque, S. T. Koshy, A. Khademhosseini, *Tissue Eng. Part A* **2011**, *17*, 1713.

[33] J. W. Nichol, S. T. Koshy, H. Bae, C. M. Hwang, S. Yamanlar, A. Khademhosseini, *Biomaterials* **2010**, *31*, 5536.

[34] S. B. Kim, K. I. Koo, H. Bae, M. R. Dokmeci, G. A. Hamilton, A. Bahinski, S. M. Kim, D. E. Ingber, A. Khademhosseini, *Lab Chip* **2012**, *12*, 3976.